Unraveling of a detailed-balance-preserved quantum master equation and continuous feedback control of a measured qubit

JunYan Luo,[1,*] Jinshuang Jin,[2] Shi-Kuan Wang,[3] Jing Hu,[1] Yixiao Huang,[1] and Xiao-Ling He[1]

[1]*Department of Physics, Zhejiang University of Science and Technology, Hangzhou 310023, China*

[2]*Department of Physics, Hangzhou Normal University, Hangzhou 310036, China*

[3]*Department of Physics, Hangzhou Dianzi University, Hangzhou 310018, China*

(Received 24 August 2015; revised manuscript received 23 January 2016; published 14 March 2016)

We present a generic unraveling scheme for a detailed-balance-preserved quantum master equation applicable for stochastic point processes in mesoscopic transport. It enables us to investigate continuous measurement of a qubit on the level of single quantum trajectories, where essential correlations between the inherent dynamics of the qubit and detector current fluctuations are revealed. Based on this unraveling scheme, feedback control of the charge qubit is implemented to achieve a desired pure state in the presence of the detailed-balance condition. With sufficient feedback strength, coherent oscillations of the measured qubit can be maintained for arbitrary qubit-detector coupling. Competition between the loss and restoration of coherence entailed, respectively, by measurement back action and feedback control is reflected in the noise power spectrum of the detector's output. It is demonstrated unambiguously that the signal-to-noise ratio is significantly enhanced with increasing feedback strength and could even exceed the well-known Korotkov-Averin bound in quantum measurement. The proposed unraveling and feedback scheme offers a transparent and straightforward approach to effectively sustaining ideal coherent oscillations of a charge qubit in the field of quantum computation.

DOI: 10.1103/PhysRevB.93.125122

I. INTRODUCTION

The advent of quantum information technologies is creating a considerable demand for strategies to manipulate individual quantum systems in the presence of noise [1]. Recently, state-of-the-art nanofabrication has made it possible to monitor a single quantum state in a continuous manner [2–5]. Broad prospects are thus attainable for physically implementing the measurement-based (closed-loop) feedback control of a quantum system in which the real-time information about the detector's output is extracted and appropriate corrections are instantaneously fed back into the system to obtain some desired behavior. Thus far, a variety of efficient quantum feedback protocols have been proposed with potentially wide-ranging applications, such as the purification of a charge qubit [6–14], the realization of a mesoscopic Maxwell's demon [15–17], and the freezing of a charge distribution [18,19] in full counting statistics [20,21]. In particular, considerable experimental progress has now been made toward the realization of the continuous feedback control of a single mesoscopic qubit [22,23], as well as of microscopic quantum systems [24–26].

In contrast to classical feedback control, which allows the acquisition of an essentially unlimited degree of specific system information, quantum feedback control involves a measured system that is inevitably disturbed in an unpredictable manner, and the availability of information is fundamentally limited by Heisenberg's uncertainty principle. The essence of the quantum measurement process involves a tradeoff between the acquisition of quantum system information and the dephasing of the measured quantum state owing to the detector's back action. The modern theory of weak quantum measurement offers the crucial possibility of deducing system information encoded in the detector's degrees of freedom in a continuous manner, which can promote a balance between information acquisition and the disturbance of the measured system.

Quantum trajectory theory has been widely considered as an appropriate description to facilitate weak continuous quantum measurements, with extensive applications in both quantum optics [27] and mesoscopic physics [28–30]. Basically, quantum trajectories are obtained via unraveling of a Lindblad quantum master equation (QME). An alternative Bayesian formalism has been shown to provide precisely equivalent results [31,32]. The unique advantages of these approaches are their clear physical implications and the simplicity with which the evolution of a quantum system can be unraveled, where system information is continuously acquired and feedback operations can be appropriately implemented [1,33]. However, it has been shown that the Lindblad QME does not necessarily satisfy the detailed-balance relation, a manifestation of the essential energy exchange between a reduced system and the detector during the measurement process [34–37]. Therefore, it is crucial to develop a means of physically unraveling the detailed-balance-preserved QME into individual quantum trajectories for enabling the continuous application of quantum feedback control.

Presently, the unraveling of a detailed-balance-preserved QME has been established only for the quantum diffusion process [38], which is thus limited to applications to a diffusive detector such as a quantum point contact (QPC). As an alternative to a QPC, a quantum-dot- (QD-) based single-electron transistor (SET) has been proposed as a sensitive qubit detector with a number of superior characteristics relative to a QPC, such as low noise, wide circuit bandwidth, and weakened temperature restrictions [39–44]. In particular, SET-based single-shot measurement has recently been realized experimentally [45,46]. As such, conduction of SET-based quantum measurements and feedback control would be highly desirable. However, in comparison with a QPC, the crucial

*jyluo@zust.edu.cn

difference of the SET detection current is that its transport characteristics are dominated by single-electron tunneling events, i.e., so-called stochastic point processes. It is therefore appealing to establish an unraveling scheme of a QME applicable to stochastic point processes of SET detectors to enable continuous quantum measurement and feedback control while unambiguously preserving the detailed balance simultaneously.

In this work, we first construct a generic scheme to unravel a detailed-balance-preserved QME for the stochastic point process of the tunneling events. It enables us to simulate single quantum trajectories, in which system information is continuously acquired and feedback control is appropriately implemented. The proposed unraveling scheme is employed to protect a desired charge qubit under continuous weak detection by an SET, with appropriate treatment of the essential energy exchange between the qubit and detector. It is clearly demonstrated that coherent oscillations of the qubit are sustained for sufficient feedback strength, and the corresponding synchronization degree can attain its maximum value. The crucial competition mechanism between measurement-induced qubit dephasing and the revival of coherence due to feedback is uniquely reflected in the detector's output noise power spectrum. It is unambiguously demonstrated that the signal-to-noise ratio can be significantly improved with increasing feedback strength and, remarkably, may even exceed the well-known Korotkov-Averin bound in quantum measurement.

The remainder of the paper is organized as follows. We begin in Sec. II with the presentation of a generic scheme for unraveling a detailed-balance-preserved QME into an ensemble of individual quantum trajectories. The proposed scheme is utilized to investigate continuous measurement of a charge qubit by an SET detector in Sec. III. The essential correlations between inherent dynamics of the qubit and detector current fluctuations are revealed in Sec. III A on the level of single quantum trajectories. Section III B is dedicated to the feedback control of the charge state based on the proposed unraveling scheme to achieve a desired pure state in the presence of the detailed-balance condition. The Korotkov-Averin bound and the conditions whereby it may be violated are discussed in Sec. III C. Finally, we summarize the work in Sec. IV.

II. UNRAVELING OF A DETAILED-BALANCE-PRESERVED QME

In this section, we develop a general scheme for unraveling a detailed-balance-preserved QME, which is applicable to stochastic point processes in a wide range of nanostructures. Let us consider a generic mesoscopic system with the total Hamiltonian given by $H = H_0(d^\dagger,d) + H_{\rm B} + H'$, where $H_0(d^\dagger,d)$ refers to the reduced quantum system of our interest with $d^\dagger$ (d) the creation (annihilation) operator of the reduced system.

The second term $H_{\rm B}$ is the Hamiltonian of the electrodes. To be more specific and without loss of generality, we consider a two-terminal device, where noninteracting electrons in the left and right electrodes are modeled by $H_{\rm B} = \sum_{\ell={\rm L,R}}\sum_k \varepsilon_{\ell k} c^\dagger_{\ell k} c_{\ell k}$, with $c^\dagger_{\ell k}$ ($c_{\ell k}$) the creation (annihilation) of an electron in the left (ℓ=L) or right (ℓ=R) electrode. Generalization to a multiterminal geometry is straightforward. The left and right reservoirs are assumed to be in local thermal equilibrium such that they can be characterized by the Fermi functions $f_{\rm L/R}(\omega) = \{1 + e^{\beta(\omega-\mu_{\rm L/R})}\}^{-1}$, where $\beta = (k_{\rm B}T)^{-1}$ is the inverse temperature, with $k_{\rm B}$ the Boltzmann constant and T the temperature. The Fermi energies of the left and right reservoirs, $\mu_{\rm L}$ and $\mu_{\rm R}$, determine the bias voltage applied across the reduced system, i.e., $V = \mu_{\rm L} - \mu_{\rm R}$. In what follows, we adopt symmetric application of the bias voltage, which means that $\mu_{\rm L/R} = \pm V/2$. Stochastic electron tunneling between the reduced system and the electrodes is depicted by $H' = \sum_\ell \{F_\ell d^\dagger + {\rm H.c.}\}$ with $F_\ell = \sum_k t_{\ell k} c_{\ell k}$ and $t_{\ell k}$ the tunneling amplitude.

The dynamics of the reduced quantum system is described by the reduced density matrix $\rho(t)$. Under the condition that the reduced system and the reservoirs are weakly coupled, the corresponding QME can be derived by tracing the entire density matrix over the reservoir's degree of freedom under a second-order cumulant expansion with respect to the tunneling Hamiltonian H' [47]. In order to achieve an accurate interpretation of the output characteristics of a device, it is instructive to decompose the reduced density matrix into particle-number-resolved ones, in which the reduced density matrices are conditioned on the number of transmitted electrons.

This can be done via decomposition of the entire Hilbert space of the electrode reservoirs [48,49]. Consider that the entire system is initially in a "vacuum" state $|0\rangle$, which means that the left and right electrodes are filled with electrons up to the Fermi energies $\mu_{\rm L}$ and $\mu_{\rm R}$, respectively. This vacuum state, however, is unstable due to the tunnel-coupling H'. It decays to a state $d^\dagger c_{{\rm L}k}|0\rangle$ with an electron in the reduced system and a hole in the left electrode. This state is also unstable and will decay to a state $c^\dagger_{{\rm R}k'} c_{{\rm L}k}|0\rangle$, having an electron in the right electrode and a hole in the left one. The state will further decay into a state $c^\dagger_{{\rm R}k'} d^\dagger c_{{\rm L}k''} c_{{\rm L}k}|0\rangle$, and so on. The evolution of the entire system is described by the following many-particle wave function [48]:

$$|\Psi(t)\rangle = \Bigg[z_0(t) + \sum_k z_{1k}(t) d^\dagger c_{{\rm L}k} + \sum_{kk'} z_{kk'}(t) c^\dagger_{{\rm R}k'} c_{{\rm L}k} + \sum_{k''<k,k'} z_{k'1k''k}(t) c^\dagger_{{\rm R}k'} d^\dagger c_{{\rm L}k''} c_{{\rm L}k} + \cdots \Bigg] |0\rangle, \quad (1)$$

where $z(t)$ are the time-dependent probability amplitudes for finding the system in the corresponding states described above. Essentially, these amplitudes are closely associated with the reduced density matrix. For instance, $\rho^{(0,0)}(t) = |z_0(t)|^2$ describes the reduced system without electron tunneling through the left and right junctions. Analogously, $\rho^{(1,0)}(t) = \sum_k |z_{1k}(t)|^2$ denotes the reduced state with one electron tunneled through the left junction and no electron through the right one; $\rho^{(1,1)}(t) = \sum_{k'k} |z_{kk'}(t)|^2$ represents the reduced state with one electron tunneled through each of the left and right junctions, respectively, and so on. Averaging over the reservoir's degrees of freedom on both sides of Eq. (1), one

arrives straightforwardly at

$$\rho(t)=\rho^{(0,0)}(t)+\rho^{(1,0)}(t)+\cdots=\sum_{N_{\rm L},N_{\rm R}}\rho^{(N_{\rm L},N_{\rm R})}(t), \quad (2)$$

where $\rho^{(N_{\rm L},N_{\rm R})}(t)$ is the so-called electron-number-resolved density matrix, describing the state of the reduced system conditioned on the event that $N_{\rm L}$ electrons were transmitted across the left and $N_{\rm R}$ across the right junction up to the time t. The time evolution of the many-particle wave function in Eq. (1) satisfies the Schrödinger equation. By partial tracing over the reservoir's degree of freedom, one eventually arrives at the following electron-number-resolved QME [48,49]:

$$\begin{aligned}\dot\rho^{(N_{\rm L},N_{\rm R})}=&-(i\mathcal{L}_0+\mathcal{R}_0)\rho^{(N_{\rm L},N_{\rm R})}-\mathcal{R}_{\rm L}^{+}\rho^{(N_{\rm L}+1,N_{\rm R})}\\&-\mathcal{R}_{\rm L}^{-}\rho^{(N_{\rm L}-1,N_{\rm R})}-\mathcal{R}_{\rm R}^{+}\rho^{(N_{\rm L},N_{\rm R}+1)}-\mathcal{R}_{\rm R}^{-}\rho^{(N_{\rm L},N_{\rm R}-1)},\end{aligned} \quad (3)$$

where $\mathcal{L}_0(\cdots)\equiv[H_0,(\cdots)]$ stands for the Liouvillian associated with the Hamiltonian H_0 of the reduced quantum system, and

$$\mathcal{R}_0\rho^{(N_{\rm L},N_{\rm R})}=\frac{1}{2}\{d^\dagger A^{(-)}\rho^{(N_{\rm L},N_{\rm R})}+\rho^{(N_{\rm L},N_{\rm R})}A^{(+)}d^\dagger\}+\text{H.c.} \quad (4a)$$

represents the continuous evolution of the reduced system. The last four terms in Eq. (3), i.e.,

$$\mathcal{R}_{\rm L}^{+}\rho^{(N_{\rm L}+1,N_{\rm R})}=-\tfrac{1}{2}\{d^\dagger\rho^{(N_{\rm L}+1,N_{\rm R})}A_{\rm L}^{(+)}\}+\text{H.c.}, \quad (4b)$$

$$\mathcal{R}_{\rm L}^{-}\rho^{(N_{\rm L}-1,N_{\rm R})}=-\tfrac{1}{2}\{A_{\rm L}^{(-)}\rho^{(N_{\rm L}-1,N_{\rm R})}d^\dagger\}+\text{H.c.}, \quad (4c)$$

$$\mathcal{R}_{\rm R}^{+}\rho^{(N_{\rm L},N_{\rm R}+1)}=-\tfrac{1}{2}\{d^\dagger\rho^{(N_{\rm L},N_{\rm R}+1)}A_{\rm R}^{(+)}\}+\text{H.c.}, \quad (4d)$$

$$\mathcal{R}_{\rm R}^{-}\rho^{(N_{\rm L},N_{\rm R}-1)}=-\tfrac{1}{2}\{A_{\rm R}^{(-)}\rho^{(N_{\rm L},N_{\rm R}-1)}d^\dagger\}+\text{H.c.}, \quad (4e)$$

describe electron tunneling through the left and right junctions of the device. Throughout this work, we set $\hbar=e=1$ for Planck's constant and the electron charge, unless stated otherwise. Equation (2) implies that the number of electrons tunneled through the left and right junctions is a stochastic variable, with the probability distribution given by $P(N_{\rm L},N_{\rm R},t)=\text{tr}\{\rho^{(N_{\rm L},N_{\rm R})}(t)\}$, where $\text{tr}\{\cdots\}$ represents the trace over the degrees of freedom of the reduced system. It is apparent that the probability distribution satisfies the normalization condition $\sum_{N_{\rm L},N_{\rm R}}P(N_{\rm L},N_{\rm R},t)=\text{tr}\{\rho(t)\}=1$. Actually, the study of the stochastic nature of mesoscopic transport is within the scope of the well-known theory of full counting statistics [20,21]. Here, we are interested in the continuous weak measurement, in which the detector acquires system information and renders the measured system in a continuous manner. This is in contrast to the project measurement, which occurs instantaneously and extracts system information completely. It is the purpose of the present work to unravel the QME into individual quantum trajectories to study the stochastic nature in quantum weak measurements. A specific example will be given in Sec. III.

In deriving Eq. (3) we have introduced $A^{(\pm)}=\sum_{\ell={\rm L,R}}A_\ell^{(\pm)}$ and $A_\ell^{(\pm)}\equiv[\tilde C_\ell^{(\pm)}(\pm\mathcal{L}_0)+i\tilde D_\ell^{(\pm)}(\pm\mathcal{L}_0)]d$, with the coupling spectral functions given by

$$\tilde C_\ell^{(\pm)}(\pm\mathcal{L}_0)=\int_{-\infty}^{\infty}dt\,C_\ell^{(\pm)}(t)e^{\pm i\mathcal{L}_0 t}. \quad (5)$$

The reservoir correlation functions involved, characterizing the effect of electron stochastic tunneling into (+) and out of (−) the device, are defined as

$$C_\ell^{(+)}(t)=\langle F_\ell^\dagger(t)F_\ell\rangle_{\rm B}, \quad (6a)$$

$$C_\ell^{(-)}(t)=\langle F_\ell(t)F_\ell^\dagger\rangle_{\rm B}, \quad (6b)$$

where $\langle\cdots\rangle_{\rm B}\equiv\text{tr}_{\rm B}[(\cdots)\rho_{\rm B}]$ stands for the trace over the local thermal equilibrium state ($\rho_{\rm B}$) of the reservoirs of the device. With the knowledge of the reservoir spectral functions, the dispersion functions $\tilde D_\ell^{(\pm)}(\pm\mathcal{L}_0)$ can be evaluated according to the Kramers-Kronig relation [50,51]

$$\tilde D_\ell^{(\pm)}(\pm\mathcal{L}_0)=-\frac{\mathcal{P}}{\pi}\int_{-\infty}^{\infty}d\omega\frac{\tilde C_\ell^{(\pm)}(\pm\omega)}{\mathcal{L}_0-\omega}, \quad (7)$$

where $\mathcal{P}$ stands for the Cauchy principal value. The dispersion functions are responsible for renormalization of the internal energy scales [52–54].

Note that the reservoir correlation functions in Eq. (6) satisfy the symmetry and detailed-balance relations as follows [47,55]:

$$[C_\ell^{(\pm)}(t)]^*=e^{\pm\beta\mu_\ell}C_\ell^{(\mp)}(t-i\beta). \quad (8)$$

According to Eq. (5), the above detailed-balance relation can be reexpressed in the frequency domain as

$$\tilde C_\ell^{(\pm)}(+\mathcal{L}_0)=e^{\pm\beta(\mu_\ell\pm\mathcal{L}_0)}\tilde C_\ell^{(\mp)}(-\mathcal{L}_0). \quad (9)$$

For large measurement voltage, i.e., where the applied voltage is much greater than the internal energy scales of the qubit, the coupling spectrum functions $\tilde C_\ell^{(\pm)}(\pm\mathcal{L}_0)$ can be well approximated by $\tilde C_\ell^{(\pm)}(0)$. Under such an approximation, our approach reduces to the conventional Lindblad QME [28,30], or, equivalently, to the quantum Bloch equations derived by Gurvitz *et al.* [42,56].

The unique advantage of the present approach is that it is able to properly account for the energy exchange between the reduced system and the reservoirs, and thus ensures the detailed-balance relation, as implied in Eq. (9). Physically, $\tilde C_\ell^{(+)}(+\mathcal{L}_0)$ is relevant to electron tunneling from the electrodes to the reduced system which is accompanied by absorption of energy quanta from the quantum system, and $\tilde C_\ell^{(-)}(-\mathcal{L}_0)$ describes the opposite process with emission of energy quanta to the quantum system. Thus, $\tilde C_\ell^{(\pm)}(\pm\mathcal{L}_0)$ imply the essential correlation between the dynamics of a reduced system and current fluctuations of the device. It is this unique feature of energy exchange between the reduced system and reservoirs that leads eventually to the detailed-balance relation in Eq. (9).

Indeed, the detailed-balance relation has important impact on the dynamics of a reduced system. Yet the power of the detailed-balance-preserved QME cannot be readily unleashed unless it can be unraveled into single quantum trajectories in which important quantum operations, such as continuous quantum measurement and quantum feedback

control, can be appropriately implemented. Furthermore, the unraveling enables us to reveal how the energy exchange affects this dynamics, in particular, the evolution of a quantum state into decoherence with only a limited number of realizations. However, unraveling of the detailed-balance-preserved QME (3) is not a trivial matter, as it actually corresponds to an infinite number of coupled equations. We thus perform a discrete Fourier transformation $\tilde{\rho}(\chi_{\rm L},\chi_{\rm R},t) = \sum_{N_{\rm L},N_{\rm R}} e^{i(N_{\rm L}\chi_{\rm L}+N_{\rm R}\chi_{\rm R})}\rho^{(N_{\rm L},N_{\rm R})}(t)$, where χ_ℓ is the so-called counting field in full counting statistics [20,21]. The transformation leads to a counting-field-dependent master equation

$$\frac{\partial}{\partial t}\tilde{\rho}(\chi_{\rm L},\chi_{\rm R},t) = \mathcal{L}_{\chi_{\rm L},\chi_{\rm R}}\tilde{\rho}(\chi_{\rm L},\chi_{\rm R},t), \tag{10a}$$

where the counting-field-dependent Liouvillian $\mathcal{L}_{\chi_{\rm L},\chi_{\rm R}}$ can be found by utilizing Eq. (3)

$$\mathcal{L}_{\chi_{\rm L},\chi_{\rm R}} = -\left\{ i\mathcal{L}_0 + \mathcal{R}_0 + \sum_{\ell={\rm L,R}}\sum_{\pm} e^{\mp i\chi_\ell}\mathcal{R}_\ell^{\pm}\right\}. \tag{10b}$$

The formal solution to Eq. (10) leads to the counting-field-dependent evolution of the system

$$\tilde{\rho}(\chi_{\rm L},\chi_{\rm R},t) = \exp\{\mathcal{L}_{\chi_{\rm L},\chi_{\rm R}}(t-t_0)\}\tilde{\rho}(\chi_{\rm L},\chi_{\rm R},t_0). \tag{11}$$

We assume that electron counting begins at t_0 such that $\rho^{(N_{\rm L},N_{\rm R})}(t_0) = \rho(t_0)\delta_{N_{\rm L},0}\delta_{N_{\rm R},0}$ and, thus, $\tilde{\rho}(\chi_{\rm L},\chi_{\rm R},t_0) = \rho(t_0)$. By performing the inverse Fourier transformation, one readily obtains the electron-number-resolved propagation of the system

$$\rho^{(N_{\rm L},N_{\rm R})}(t) = \mathcal{U}(N_{\rm L},N_{\rm R},t-t_0)\rho(t_0), \tag{12a}$$

where $\mathcal{U}(N_{\rm L},N_{\rm R},\delta t)$ is nothing but the electron-number-resolved propagator, given by

$$\mathcal{U}(N_{\rm L},N_{\rm R},\delta t) = \int_{-\pi}^{\pi}\frac{d\chi_{\rm L}d\chi_{\rm R}}{(2\pi)^2}e^{\mathcal{L}_{\chi_{\rm L},\chi_{\rm R}}\delta t - i\sum_\ell N_\ell\chi_\ell}. \tag{12b}$$

An important feature of this propagator is that it solely depends on the dynamic structure of the QME (3) rather than on the initial quantum state, which makes it very efficient for unraveling the QME (3) into individual quantum trajectories.

Specifically, let us consider the evolution of the quantum state during an infinitesimal time interval $[t_k,t_k+dt]$. In general, Eq. (12) is valid for an arbitrary number of electrons ($N_{\rm L/R}$) transmitted through the reduced system, depending on the time interval (dt). In what follows, we are interested in the stochastic point process, i.e., where individual electron tunneling events dominate. For that purpose, it is necessary to take $dt \ll \min(\Gamma_{\rm L}^{-1},\Gamma_{\rm R}^{-1})$, where Γ_ℓ is the tunnel-coupling strength between the reduced system and the left (ℓ=L) or right (ℓ=R) electrode. It ensures that the probability of having $N_\ell \geqslant 2$ electrons tunneled through the junction ℓ is practically zero. Furthermore, instead of using $N_{\rm L}$ and $N_{\rm R}$ directly, we introduce two stochastic point variables $dN_{\rm L}(t)$ and $dN_{\rm R}(t)$ to respectively represent the numbers of electrons having tunneled through the left and right junctions during the time interval dt. Given the state condition $\rho(t_k)$ at t_k, the state at t_k+dt is determined according to Eq. (12) as

$$\rho^{(dN_{\rm L},dN_{\rm R})}(t_k+dt) = \mathcal{U}(dN_{\rm L},dN_{\rm R},dt)\rho(t_k). \tag{13}$$

If the individual measurement records are ignored (i.e., averaged over), the ensemble-averaged quantum state is given by

$$\begin{aligned}\rho(t_k+dt) &= \sum_{dN_{\rm L},dN_{\rm R}}\rho^{(dN_{\rm L},dN_{\rm R})}(t_k+dt)\\ &= \sum_{dN_{\rm L},dN_{\rm R}}{\rm Pr}(dN_{\rm L},dN_{\rm R})\rho^{\rm c}(t_k+dt),\end{aligned} \tag{14}$$

where ${\rm Pr}(dN_{\rm L},dN_{\rm R}) = {\rm tr}\{\rho^{(dN_{\rm L},dN_{\rm R})}(t_k+dt)\}$ represents the probability of $dN_{\rm L}$ electrons tunneling through the left junction and $dN_{\rm R}$ electrons tunneling through the right junction at time t_k+dt, and ${\rm tr}\{\cdots\}$ denotes the trace over the degrees of freedom of the reduced system. The normalized state conditioned on a definite measurement result obtained at t_k+dt can be established from Eq. (14):

$$\rho^{\rm c}(t_k+dt) = \frac{\rho^{(dN_{\rm L},dN_{\rm R})}(t_k+dt)}{{\rm Pr}(dN_{\rm L},dN_{\rm R})}, \tag{15}$$

where the superscript "c" attached to the density matrix is to specify that the state is conditioned on the definite measurement result.

Equations (13) and (15) indicate that, if one generates $dN_{\rm L}$ and $dN_{\rm R}$ stochastically for each time interval $[t_k,t_k+dt]$ and then collapses the system onto a specific state $\rho^{\rm c}(t_k+dt)$ at the end of the time interval, one has actually achieved a particular single realization of continuous measurements conditioned on the specific measurement results. In each time interval, the stochastic point variables $dN_{\rm L}$ and $dN_{\rm R}$ are generated in such a way that their ensemble averages over a large number of quantum trajectories, denoted by $\mathrm{E}[\cdots]$, satisfy

$$\mathrm{E}[dN_{\rm L}(t)] = \Gamma_{\rm L}{\rm tr}\{d^\dagger\rho^{\rm c}(t)d\}dt, \tag{16a}$$

$$\mathrm{E}[dN_{\rm R}(t)] = \Gamma_{\rm R}{\rm tr}\{d\rho^{\rm c}(t)d^\dagger\}dt. \tag{16b}$$

It is now clear that electron tunneling conditions the future evolution of the quantum state [Eqs. (13) and (15)], while the real-time quantum state affects the observed tunneling events through the left and right junctions [cf. Eq. (16)]. Within this unraveling scheme one is able to propagate the conditioned quantum state $\rho^{\rm c}(t)$ and the observed result [$dN_{\rm L}(t)$ and $dN_{\rm R}(t)$] in a self-consistent manner.

III. APPLICATION TO QUANTUM MEASUREMENT AND FEEDBACK CONTROL

So far, we have successfully constructed an efficient scheme to unravel a detailed-balance-preserved QME into single quantum trajectories. The proposed theory is applicable to a wide range of mesoscopic systems in which transport is dominated by stochastic point process. In this section, we first investigate the conditional dynamics of a charge qubit under continuous measurement by an SET detector. The developed scheme allows us to analyze the influence of energy exchange between the qubit and detector, as well as the essential correlation between current fluctuations in the detector and qubit dynamics on the level of a single quantum trajectory. Feedback control of the charge qubit is implemented in single quantum trajectories to protect a desired pure state. The effect of feedback control is characterized by the signal-to-noise

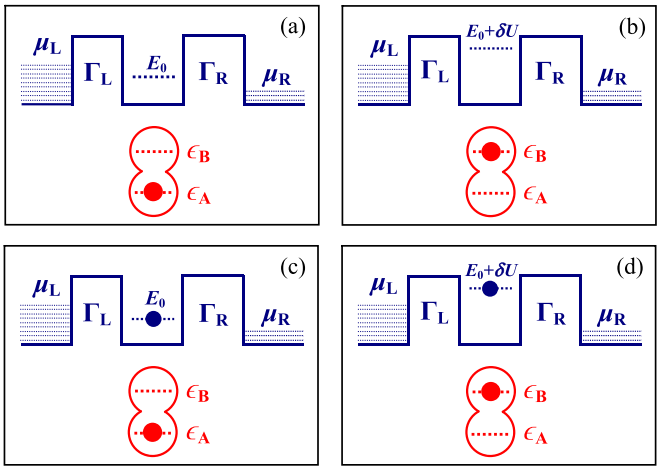

FIG. 1. Schematic setup of a solid-state charge qubit under continuous monitoring by an SET detector. The charge qubit is represented as an extra electron confined in a double QD. The SET is a single QD sandwiched between the left and right electrodes with intrinsic tunneling widths Γ_L and Γ_R, where the QD is capacitively coupled to the qubit via Coulomb repulsion. The possible electron configurations of the quantum system (qubit plus SET QD) are displayed in (a)–(d).

ratio, which might even exceed the well-known Korotkov-Averin bound in quantum measurement.

A. Continuous measurement of a qubit by an SET

A charge qubit under continuous monitoring by an SET detector is schematically shown in Fig. 1. The qubit is denoted as an extra electron in a double QD. The occupations of the extra electron in the lower and upper QDs respectively correspond to logic (dot) states $|\mathrm{A}\rangle$ and $|\mathrm{B}\rangle$ of the charge qubit. The SET detector is a single QD sandwiched between left and right electrodes of respective intrinsic tunneling widths Γ_L and Γ_R, where the QD is capacitively coupled to the qubit via Coulomb interaction. The energy level of the single QD is susceptible to changes in the nearby electrostatic environment, and, thus, can be used to sense the location of the extra electron in the charge qubit. The reduced system is comprised of the charge qubit, a single QD of the SET, and their coupling, with Hamiltonian given by

$$H_S = \tfrac{1}{2}\epsilon\,\sigma_z + \Omega\,\sigma_x + (E_0 + \delta U\,|\mathrm{B}\rangle\langle\mathrm{B}|)d^\dagger d, \qquad (17)$$

where $d^\dagger$ and d are respectively the creation and annihilation operators for an electron in the single QD, ϵ is the qubit level mismatch, Ω is the qubit interdot tunnel coupling, and $\sigma_z \equiv |\mathrm{A}\rangle\langle\mathrm{A}| - |\mathrm{B}\rangle\langle\mathrm{B}|$ and $\sigma_x \equiv |\mathrm{A}\rangle\langle\mathrm{B}| + |\mathrm{A}\rangle\langle\mathrm{B}|$ are pseudospin operators for the qubit. We assume there is only a single energy level E_0 within the bias regime defined by the Fermi energies of the left and right electrodes. If the qubit dwells in logic state $|\mathrm{B}\rangle$, the SET QD responds to the strong Coulomb repulsion δU. As a result, electron transport through the SET will be significantly affected. It is precisely this mechanism that enables the acquisition of qubit information via the readout characteristics of the SET.

Figure 2 presents particular single realizations based on the unraveling scheme developed in Sec. II. The conditional reduced density matrix element ρ^c_{jj} with $j = \{\mathrm{a,b,c,d}\}$ corresponds to the electron configurations shown in Figs. 1(a)–1(d),

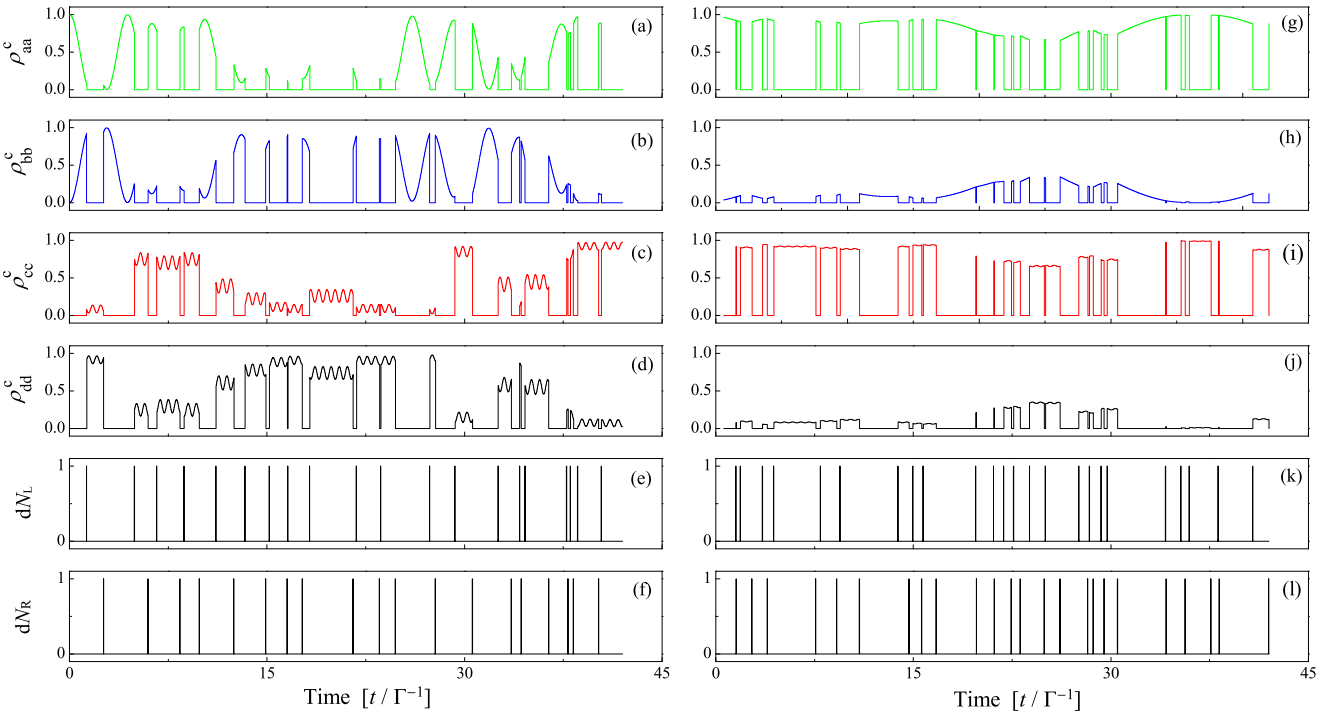

FIG. 2. Typical quantum trajectories and corresponding detection records for $\Omega/\Gamma = 1.0$ (a)–(f) and $\Omega/\Gamma = 0.1$ (g)–(l), where $\Gamma = \Gamma_L + \Gamma_R$ is held constant and used as the unit of energy. The initial condition is an empty SET QD with the charge qubit in the logic state $|\mathrm{A}\rangle$, as shown in Fig. 1(a), i.e., $\rho^c(t=0) = |\mathrm{a}\rangle\langle\mathrm{a}|$. The measurement voltage is $V/\Gamma = 3.0$, which implies $\mu_{L/R} = \pm 1.5\Gamma$. The time step used is $\Delta t = 0.01\Gamma^{-1}$. Other plotting parameters are $\epsilon = 0$, $k_B T/\Gamma = 1.0$, $\Gamma_L = \Gamma_R = \Gamma/2$, and $\delta U/\Gamma = 10$.

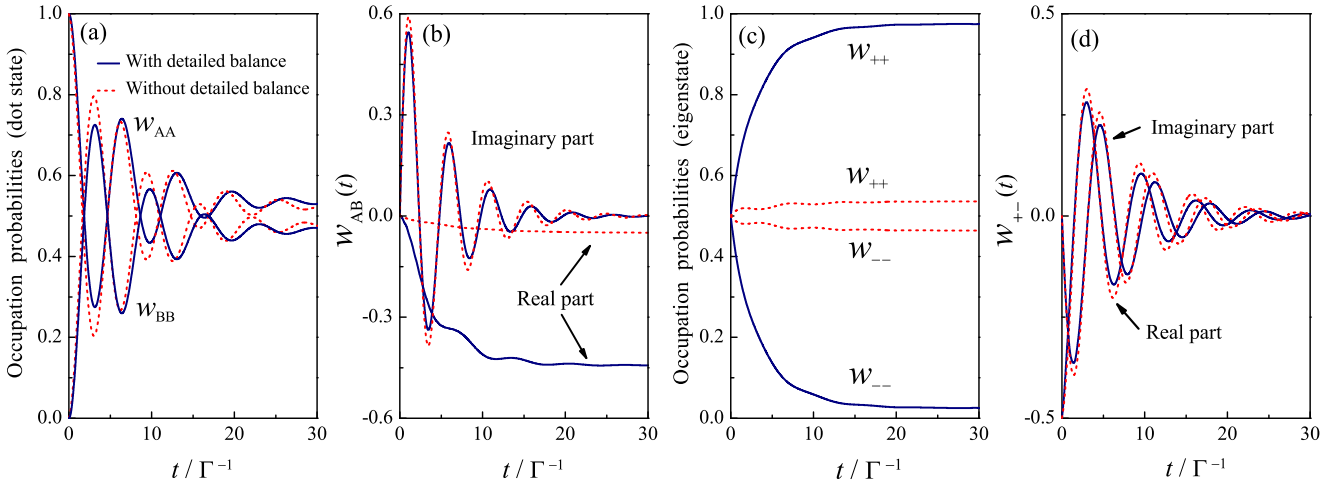

FIG. 3. Dynamics of the measured charge qubit in the dot state representation (a),(b) and eigenstate representation (c),(d), obtained by an ensemble average taken over 20 000 quantum trajectories. For comparison, the results in the absence of the detailed balance are also plotted by the dotted curves. The initial condition is $w_{AA}(t=0)=1$. The total tunneling width $\Gamma=\Gamma_L+\Gamma_R$ is kept constant and used as the unit of energy. The tunnel couplings to the left and right electrodes are asymmetric, $\Gamma_L/\Gamma_R=\frac{1}{9}$. The interdot coupling of the qubit is $\Omega/\Gamma=0.5$. The other plotting parameters used are the same as those in Fig. 2.

respectively. The initial condition corresponds to the charge configuration shown in Fig. 1(a), i.e., $\rho^c(t=0)=|a\rangle\langle a|$. The single realization for $\Omega/\Gamma=1.0$ is plotted in Figs. 2(a)–2(f). The charge qubit exhibits oscillations between quantum states $|a\rangle$ and $|b\rangle$, which is stochastically interrupted whenever an electron tunnels into the SET [see, for example, Fig. 2(e) for dN_L]. The electron may dwell in the SET for a random period of time, where it experiences rapid oscillations before it tunnels out of the QD.

The single realization for a suppressed interdot coupling ($\Omega/\Gamma=0.1$) is displayed in Figs. 2(g)–2(l). Contrary to the case of $\Omega/\Gamma=0.1$, one observes very slow oscillations between $|a\rangle$ and $|b\rangle$, as shown in Figs. 2(g) and 2(h). Furthermore, one finds unambiguous examples of the bunching of electron tunneling events through the SET; see Figs. 2(k)–2(l). While the qubit stays in the logic state $|B\rangle$, it prevents electrons from tunneling through the SET due to the strong Coulomb repulsion between the qubit and the SET QD ($\delta U/\Gamma\gg 1$). Electrons can flow only over short time windows when the qubit relaxes to the logic state $|A\rangle$, leading eventually to the bunching of tunneling events. It thus clearly demonstrates that our unraveling scheme offers an essential method to reveal the correlation between the inherent dynamics of a qubit and detector current fluctuations on the level of single quantum trajectories.

Furthermore, the quantum trajectory based on the detailed-balance-preserved QME enables us to reveal the essential effect of energy exchange between the charge qubit and detector: the qubit evolves into decoherence with only a limited number of realizations. For that purpose, we investigate the unconditional evolution of the reduced system $\rho(t)$ (qubit plus SET QD) by ensemble averaging over quantum trajectories analogous to those in Fig. 2. The dynamics of the charge qubit alone $w(t)$ can then be obtained as

$$w(t)=\mathrm{tr}_{\mathrm{SET}}\{\rho(t)\}, \tag{18}$$

where $\mathrm{tr}_{\mathrm{SET}}\{\cdots\}$ stands for the trace over the degrees of freedom of the SET QD. In the charge configurations as shown in Fig. 1, one readily verifies that $w_{AA}=\rho_{aa}+\rho_{cc}$ and $w_{BB}=\rho_{bb}+\rho_{dd}$, which represent the probabilities of finding the charge qubit in the logic states $|A\rangle$ and $|B\rangle$, respectively. The nondiagonal element $w_{AB}=\rho_{ab}+\rho_{cd}$ stands for the so-called quantum coherence between logic states $|A\rangle$ and $|B\rangle$.

The numerical results are displayed in Fig. 3, where the dynamics of the charge qubit alone is obtained by ensemble averaging over 20 000 quantum trajectories (solid curves). For a close comparison, we have also presented in Fig. 3 the results in the absence of detailed balance (dotted curves), which are obtained simply by replacing $C^{(\pm)}(\pm\mathcal{L}_0)$ with $C^{(\pm)}(0)$, or equivalently using the Lindblad master equation in Refs. [30,42]. We consider very asymmetrical tunnel coupling strengths ($\Gamma_L/\Gamma_R=\frac{1}{9}$) where the measurement was found to be highly effective [42]. In the dot state representation, the relaxation behaviors are quantitatively similar; see Fig. 3(a). The measurement back-action-induced qubit dephasing behavior, characterized by the off-diagonal element of the density matrix (w_{AB}), exhibits very different behavior; see Fig. 3(b). In the absence of detailed balance, the off-diagonal element nearly vanishes in the stationary limit. However, in the presence of detailed balance, the real part of w_{AB} apparently attains a nonzero constant value.

In the eigenstate ($|+\rangle$ and $|-\rangle$) representation, nondiagonal elements of the density matrix (w_{+-} and w_{-+}) vanish in the long-time limit [57,58], regardless of whether the detailed-balance relation is satisfied or not [see Fig. 3(d)]. The qubit relaxation behavior, however, exhibits remarkable differences. The probabilities of the two eigenstates show radical differences with and without detailed balance; see Fig. 3(c). It thus clearly illustrates that our quantum trajectory theory fully accounts for the detailed-balance condition and its essential ramifications in the measurement dynamics.

B. Implementation of feedback control

We have successfully unraveled a detailed-balance-preserved QME in the context of a charge qubit under

continuous measurement by an SET. It paves the way toward feedback control of a quantum state in the presence of essential energy exchange between the quantum system and detector. We are now in a position to implement feedback control for the coherent evolution of a charge qubit based on the single realizations obtained in Sec. III A. In the dot state representation of the qubit ($|\mathrm{A}\rangle$ and $|\mathrm{B}\rangle$), the desired (target) pure state to be protected is

$$|\psi_d(t)\rangle = \cos(\Omega t)|\mathrm{A}\rangle + i\sin(\Omega t)|\mathrm{B}\rangle. \tag{19}$$

The basis of the feedback control begins by converting the detector's output information into the evolution of the qubit state $w^{\mathrm{c}}(t)$, where $w^{\mathrm{c}}(t) = \mathrm{tr}_{\mathrm{SET}}\{\rho^{\mathrm{c}}(t)\}$. The real-time qubit state $w^{\mathrm{c}}(t)$ is then compared with the target state $w_d(t) \equiv |\psi_d(t)\rangle\langle\psi_d(t)|$, and their difference is utilized to design the feedback Hamiltonian such that the difference is decreased at the next step. At each successive step, the feedback Hamiltonian acts only for an infinitesimal time interval dt. According to the suboptimal algorithm [59], state propagation in each infinitesimal time step maximizes the fidelity of $w^{\mathrm{c}}(t)$ with $w_d(t)$. Specifically, let us consider state evolution with respect to the feedback Hamiltonian H_{fb}, where the state $w^{\mathrm{c}}(t+dt)$ is given by

$$\begin{aligned} w^{\mathrm{c}}(t+dt) = {} & w^{\mathrm{c}}(t) - i[H_{\mathrm{fb}}, w^{\mathrm{c}}(t)]dt \\ & - \tfrac{1}{2}[H_{\mathrm{fb}},[H_{\mathrm{fb}}, w^{\mathrm{c}}(t)]](dt)^2 + \cdots . \end{aligned} \tag{20}$$

Here, H_{fb} is to be determined via the fidelity of the state $w^{\mathrm{c}}(t+dt)$ with the target state, defined as

$$\begin{aligned} \mathcal{F} \equiv & \langle\psi_d|w^{\mathrm{c}}(t+dt)|\psi_d\rangle \\ = & \langle\psi_d|w^{\mathrm{c}}(t)|\psi_d\rangle - i\langle\psi_d|[H_{\mathrm{fd}}, w^{\mathrm{c}}(t)]|\psi_d\rangle dt \\ & - \tfrac{1}{2}\langle\psi_d|[H_{\mathrm{fb}},[H_{\mathrm{fb}}, w^{\mathrm{c}}(t)]]|\psi_d\rangle(dt)^2 + \cdots . \end{aligned} \tag{21}$$

To optimize the fidelity, one should maximize the dominant term, i.e., the term proportional to dt. This imposes certain constraints, e.g., constraints on the sum of the squares of the eigenvalues, on the sum of the norms of the eigenvalues, or on the maximum eigenvalue of H_{fb}, which originate from either a limitation on the feedback strength or finite Hamiltonian resources. Here, employing the first type of constraint, i.e., $\mathrm{tr}_{\mathrm{qb}}\{H_{\mathrm{fb}}^2\} \leqslant \nu$, where ν is the feedback strength and $\mathrm{tr}_{\mathrm{qb}}\{\cdots\}$ represents the trace over the degrees of freedom of the charge qubit, the feedback Hamiltonian is constructed as [38,60]

$$H_{\mathrm{fb}} = i\kappa[|\psi_d(t)\rangle\langle\psi_d(t)|, w^{\mathrm{c}}(t)], \tag{22}$$

where $\kappa = \sqrt{\frac{\nu}{2(p-q)}}$, with $p = \langle\psi_d|[w^{\mathrm{c}}(t)]^2|\psi_d\rangle$ and $q = [\langle\psi_d|w^{\mathrm{c}}(t)|\psi_d\rangle]^2$.

It is also instructive to insert the target state [Eq. (19)] into Eq. (22), which provides

$$H_{\mathrm{fb}} = K\sigma_x \tag{23a}$$

with σ_x the pseudospin operator for the charge qubit defined in Eq. (17) and

$$K = \begin{cases} +\sqrt{\frac{\nu}{2}}, & \Delta\phi < 0, \\ -\sqrt{\frac{\nu}{2}}, & \Delta\phi > 0. \end{cases} \tag{23b}$$

This, in fact, yields another version of H_{fb} that resembles a simple bang-bang control. The feedback parameter between two values is readily determined by the phase error defined as $\Delta\phi \equiv \phi(t) - \phi_0$, where $\phi(t) = \arctan\left(2\mathrm{Im}\{w^{\mathrm{c}}_{\mathrm{AB}}(t)\}/[w^{\mathrm{c}}_{\mathrm{AA}}(t) - w^{\mathrm{c}}_{\mathrm{BB}}(t)]\right)$ represents the relative phase between states $|\mathrm{A}\rangle$ and $|\mathrm{B}\rangle$, and $\phi_0 = 2\Omega t (\mathrm{mod}\ 2\pi)$. It is noted that the two versions of H_{fb} given by Eqs. (22) and (23) are completely equivalent. Yet the unique advantage of the latter version is that it is much easier to implement experimentally.

The effect of feedback control is plotted in Fig. 4 for various values of feedback strength ν. The feedback is implemented in each quantum trajectory, analogous to those shown in Fig. 2. The propagation of the state is obtained from an ensemble average over 20 000 trajectories. For a sufficiently large feedback strength (see the dotted curves for $\nu = 1$), coherent oscillations of the charge qubit can be maintained, in principle,

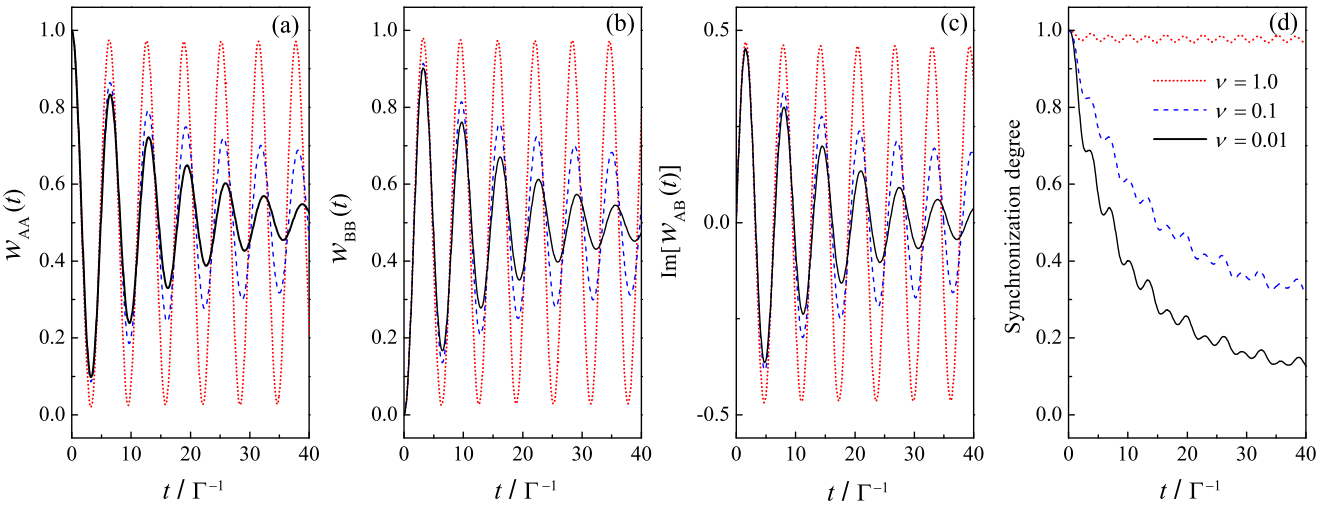

FIG. 4. Time evolution of the charge qubit and corresponding synchronization degree for various values of feedback strength ν: 0.01 (solid curves), 0.1 (dashed curves), and $\nu = 1.0$ (dotted curves). The results are obtained from the ensemble average over 20 000 quantum trajectories. The inherent qubit interdot coupling is $\Omega/\Gamma = 0.5$, where $\Gamma = \Gamma_{\mathrm{L}} + \Gamma_{\mathrm{R}}$ is held constant, and is used as the unit of energy. All other plotting parameters are equivalent to those employed in Fig. 2.

for an arbitrary period of time. To quantitatively characterize how close to the desired state the protected state could come, we introduce the synchronization degree, defined as $D \equiv 2\langle \mathrm{tr}_{\mathrm{qb}}\{w^{c} w_{d}\}\rangle - 1$, with $\langle \cdots \rangle$ the time average. Complete synchronization exists for $D = 1$, indicating that the target state is perfectly sustained via the feedback control. The results for the various feedback strengths considered are shown in Fig. 4(d). Apparently, for $\nu = 1$, D comes very close to the maximum value of 1, verifying thus the high effectiveness of our feedback scheme.

C. Signal-to-noise ratio

The essence of the continuous quantum measurement process involves the tradeoff between the acquisition of qubit information and the back-action-induced dephasing of the qubit [56,61–63]. Feedback control serves as an essential mechanism to restore the coherence of the quantum state. To characterize the competition between the back-action-induced dephasing and feedback-control-induced revival of coherence, it is instructive to investigate the noise power spectrum $S(\omega)$ of the detector's output, which is defined as the Fourier transform of the two-time correlation function $G(\tau)$ of the detection current:

$$S(\omega) = 2\int_{-\infty}^{\infty} d\tau\, e^{i\omega\tau} G(\tau). \tag{24}$$

Here, according to quantum trajectory theory, $G(\tau)$ is given by [29,64]

$$G(\tau) = \{\mathrm{E}[i_{\ell}(t+\tau) i_{\ell}(t)] - \mathrm{E}[i_{\ell}(t+\tau)]\mathrm{E}[i_{\ell}(t)]\}|_{t\to\infty}, \tag{25}$$

where $i_{\ell}(t) = dN_{\ell}/dt$ is the stochastic current through the left ($\ell = \mathrm{L}$) or right ($\ell = \mathrm{R}$) junction for the stochastic point process.

Let us first evaluate $G(\tau)$ for the current transport through the left junction of the SET (the right junction provides the same results, as we have verified), which qualitatively characterizes the influence of the quantum feedback control on the measurement dynamics. Figure 5 presents numerical results for $G(\tau)$ for various values of feedback strength ν, where ensemble averages are obtained over 20 000 quantum trajectories. For a small feedback strength ($\nu = 0.01$), the quantum system gradually loses its correlation, as shown in Fig. 5(a). As feedback strength increases, the correlation function clearly demonstrates coherent oscillation behavior; see Fig. 5(c) for $\nu = 1.0$.

With an adequate knowledge of $G(\tau)$, it is straightforward to obtain $S(\omega)$ using Eq. (24). Here, to obtain a smooth representation of $G(\tau)$, 80 000 more quantum trajectories were used. The influence of feedback control on $S(\omega)$ for values of ν defined as 0.01 (solid curves), 0.1 (dashed curves), and 1.0 (dotted curves) is displayed in Fig. 6. All other parameters are equivalent to those employed for Fig. 5. The most important feature is a noise peak located at the qubit characteristic frequency $\Delta = \sqrt{\epsilon^2 + 4\Omega^2}$, which is in fact a reflection of the coherent oscillations of the qubit. Interestingly, the height of this peak [$S(\Delta)$] relative to its noise pedestal, given as $S_{\infty} = S(\infty)$, has been shown to be a measure of the signal-to-noise ratio (SNR) [65,66]

$$\mathrm{SNR} = \frac{S(\Delta) - S_{\infty}}{S_{\infty}}. \tag{26}$$

The signal-to-noise ratio characterizes how close to the quantum limit the detector can operate. It has been argued that the tradeoff between the acquisition of qubit information and the back-action-induced dephasing leads to a fundamental limit on the SNR, which is well known as the Korotkov-Averin bound in quantum measurement [65,66]. According to this limit, the SNR can have a maximum value of 4, which can occur only for

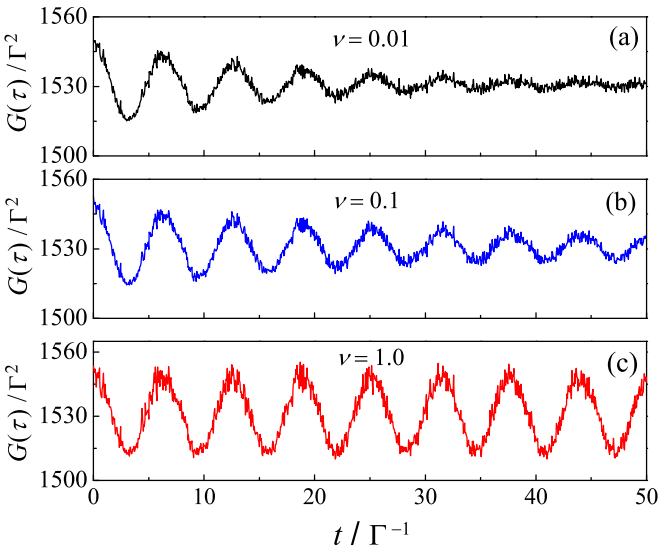

FIG. 5. Correlation functions $G(\tau)$ of the detection current through the left junction for various values of feedback strength: (a) $\nu = 0.01$; (b) $\nu = 0.1$; and (c) $\nu = 1.0$. The correlation functions are obtained from ensemble averages over 20,000 quantum trajectories. All other plotting parameters are equivalent to those employed in Fig. 4.

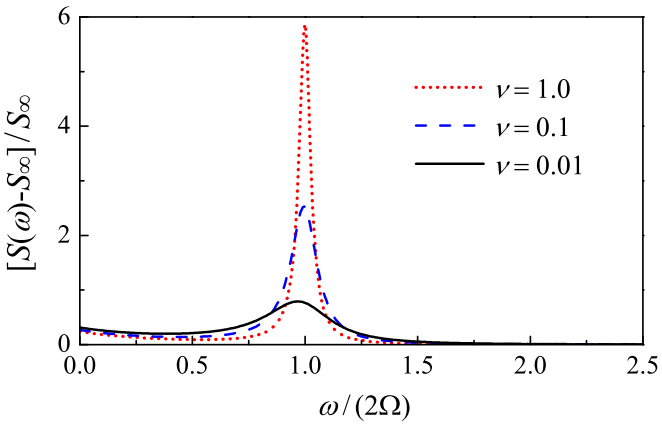

FIG. 6. Noise power spectrum of the detection current through the left junction obtained by Fourier transform of the corresponding correlation functions for various values of feedback strength: $\nu = 0.01$ (solid curve); $\nu = 0.1$ (dashed curve); and $\nu = 1.0$ (dotted curve). To obtain a smooth representation of the correlation functions, 80,000 more quantum trajectories were used. Other parameters are the same as those in Fig. 5.

a quantum-limited detector, where the qubit loses coherence purely due to the flow of qubit information, rather than due to fluctuating environments. In a less effective measurement, qubit dephasing occurs faster than the information acquisition, and the resultant SNR is less than 4.

It has been argued that the SNR of an SET detector cannot attain the limit of an ideal detector [42]. We find consistent results for a weak feedback strength ($\nu = 0.01$), as shown by the solid curve in Fig. 6. However, with an increasing feedback strength, coherence of the charge qubit is effectively restored, which leads to a prominent rise in the coherent peak. Remarkably, in the case of strong feedback strength (see the dotted curve in Fig. 6 for $\nu = 1.0$) we observe an SNR greater than the bound limit of 4, leading to a violation of the Korotkov-Averin bound. Our proposed feedback protocol therefore serves as an effective method to improve the SNR and restore ideal coherent oscillations of a qubit under continuous measurement by an SET detector.

So far, a variety of approaches have been proposed that can potentially result in the violation of the Korotkov-Averin bound. These approaches are basically divided into two types. The first type is based on the inhibition of the noise pedestal using strongly responding detectors [43,44] or twin detectors [67,68]. The second type involves the restoration of the coherence of the qubit by utilizing, for example, quantum nondemolition measurements [69,70] or the non-Markovian memory effect [71]. The violation of the Korotkov-Averin bound in the present work belongs to the second type. The unique advantage of this approach is that we can precisely achieve a desired SNR in a controllable manner by simply adjusting the feedback strength.

Recently, an SET-detection-based feedback scheme has also been proposed for the stabilization of a pure state, where electronic detector current is directly back coupled into the qubit parameter [11]. It was demonstrate that charge qubit states are stabilized above a critical detector-qubit coupling simply after a few electron jumps through the detector. In comparison, the advantage of the present feedback scheme is that coherent oscillations of the qubit can be maintained, in principle, for arbitrary qubit-SET coupling parameters, provided the feedback is sufficiently strong.

IV. SUMMARY

We have developed a generic and efficient scheme for the unraveling of a detailed-balance-preserved quantum master equation. It is applicable to a wide range of nanostructures in which transport is dominated by stochastic point processes. The proposed scheme was employed to investigate continuous measurement of a charge qubit by a single-electron transistor, where essential correlations between the inherent dynamics of the qubit and detector current fluctuations were revealed on the level of single quantum trajectories. It was illustrated that energy exchange between the detector and qubit has a vital role to play in the measurement dynamics, particularly in the decoherence behavior of the charge qubit. The quantum trajectory enables us to implement feedback control of the charge state to achieve a desired pure state in the presence of the detailed-balance condition. It was demonstrated that coherent oscillations of the charge qubit can be maintained for an arbitrary period of time, and the corresponding synchronization degree can attain its maximum value for sufficient feedback strength. The effectiveness of the feedback control was further reflected in the noise power spectrum of the detector's output. The signal-to-noise ratio was observed to increase with rising feedback strength, and, remarkably, could even exceed the well-known Korotkov-Averin bound in quantum measurement. The proposed unraveling scheme together with the feedback control algorithm turned out to be effective in protecting and maintaining ideal quantum coherent oscillations in a very transparent and straightforward manner, and thus are anticipated to have important applications in the field of solid-state quantum computation.

ACKNOWLEDGMENTS

We would like to thank Lingzhen Guo for fruitful discussions and suggestions. Support from the National Natural Science Foundation of China (Grants No. 11204272 and No. 11274085) and the Natural Science Foundation of Zhejiang Province (Grants No. LY15A040007, No. LY15A040006, and No. LZ13A040002) is gratefully acknowledged.

[1] H. M. Wiseman and G. J. Milburn, *Quantum Measurement and Control* (Cambridge University Press, Cambridge, 2010).
[2] T. Fujisawa, T. Hayashi, R. Tomita, and Y. Hirayama, Science **312**, 1634 (2006).
[3] Y. Yu, S.-L. Zhu, G. Sun, X. Wen, N. Dong, J. Chen, P. Wu, and S. Han, Phys. Rev. Lett. **101**, 157001 (2008).
[4] S. Gustavsson, R. Leturcq, M. Studer, I. Shorubalko, T. Ihn, K. Ensslin, D. Driscoll, and A. Gossard, Surf. Sci. Rep. **64**, 191 (2009).
[5] R. Vijay, D. H. Slichter, and I. Siddiqi, Phys. Rev. Lett. **106**, 110502 (2011).
[6] H. M. Wiseman, S. Mancini, and J. Wang, Phys. Rev. A **66**, 013807 (2002).
[7] R. Ruskov and A. N. Korotkov, Phys. Rev. B **66**, 041401 (2002).
[8] A. N. Korotkov, Phys. Rev. B **71**, 201305 (2005).
[9] A. N. Jordan and A. N. Korotkov, Phys. Rev. B **74**, 085307 (2006).
[10] E. J. Griffith, C. D. Hill, J. F. Ralph, H. M. Wiseman, and K. Jacobs, Phys. Rev. B **75**, 014511 (2007).
[11] G. Kießlich, G. Schaller, C. Emary, and T. Brandes, Phys. Rev. Lett. **107**, 050501 (2011).
[12] C. Pöltl, C. Emary, and T. Brandes, Phys. Rev. B **84**, 085302 (2011).
[13] G. Kießlich, C. Emary, G. Schaller, and T. Brandes, New J. Phys. **14**, 123036 (2012).
[14] W. Kopylov, C. Emary, E. Schöll, and T. Brandes, New J. Phys. **17**, 013040 (2015).
[15] G. Schaller, C. Emary, G. Kiesslich, and T. Brandes, Phys. Rev. B **84**, 085418 (2011).

[16] P. Strasberg, G. Schaller, T. Brandes, and M. Esposito, Phys. Rev. Lett. **110**, 040601 (2013).
[17] M. Esposito and G. Schaller, EPL (Europhys. Lett.) **99**, 30003 (2012).
[18] T. Brandes, Phys. Rev. Lett. **105**, 060602 (2010).
[19] S. Daryanoosh, H. M. Wiseman, and T. Brandes, Phys. Rev. B **93**, 085127 (2016).
[20] Y. M. Blanter and M. Büttiker, Phys. Rep. **336**, 1 (2000).
[21] *Quantum Noise in Mesoscopic Physics*, edited by Y. V. Nazarov (Kluwer Academic Publishers, Dordrecht, 2003).
[22] R. Vijay, C. Macklin, D. H. Slichter, S. J. Weber, K. W. Murch, R. Naik, A. N. Korotkov, and I. Siddiqi, Nature (London) **490**, 77 (2012).
[23] S. Brakhane, W. Alt, T. Kampschulte, M. Martinez-Dorantes, R. Reimann, S. Yoon, A. Widera, and D. Meschede, Phys. Rev. Lett. **109**, 173601 (2012).
[24] G. G. Gillett, R. B. Dalton, B. P. Lanyon, M. P. Almeida, M. Barbieri, G. J. Pryde, J. L. O'Brien, K. J. Resch, S. D. Bartlett, and A. G. White, Phys. Rev. Lett. **104**, 080503 (2010).
[25] M. Koch, C. Sames, A. Kubanek, M. Apel, M. Balbach, A. Ourjoumtsev, P. W. H. Pinkse, and G. Rempe, Phys. Rev. Lett. **105**, 173003 (2010).
[26] C. Sayrin, I. Dotsenko, X. Zhou, B. Peaudecerf, T. Rybarczyk, S. Gleyzes, P. Rouchon, M. Mirrahimi, H. Amini, M. Brune *et al.*, Nature (London) **477**, 73 (2011).
[27] M. B. Plenio and P. L. Knight, Rev. Mod. Phys. **70**, 101 (1998).
[28] H. S. Goan, G. J. Milburn, H. M. Wiseman, and H. B. Sun, Phys. Rev. B **63**, 125326 (2001).
[29] H. S. Goan and G. J. Milburn, Phys. Rev. B **64**, 235307 (2001).
[30] H.-S. Goan, Phys. Rev. B **70**, 075305 (2004).
[31] A. N. Korotkov, Phys. Rev. B **60**, 5737 (1999).
[32] A. N. Korotkov, Phys. Rev. B **63**, 115403 (2001).
[33] K. Jacobs, *Quantum Measurement Theory and Its Applications* (Cambridge University Press, Cambridge, 2014).
[34] G. Lindblad, Rep. Math. Phys. **10**, 393 (1976).
[35] Y. J. Yan, F. Shuang, R. X. Xu, J. X. Cheng, X. Q. Li, C. Yang, and H. Y. Zhang, J. Chem. Phys. **113**, 2068 (2000).
[36] X. Q. Li, P. Cui, and Y. J. Yan, Phys. Rev. Lett. **94**, 066803 (2005).
[37] X. Q. Li, W. K. Zhang, P. Cui, J. S. Shao, Z. S. Ma, and Y. J. Yan, Phys. Rev. B **69**, 085315 (2004).
[38] S.-K. Wang, J. S. Jin, and X.-Q. Li, Phys. Rev. B **75**, 155304 (2007).
[39] M. H. Devroret and R. J. Schoelkopf, Nature (London) **406**, 1039 (2000).
[40] A. A. Clerk, S. M. Girvin, A. K. Nguyen, and A. D. Stone, Phys. Rev. Lett. **89**, 176804 (2002).
[41] D. Mozyrsky, I. Martin, and M. B. Hastings, Phys. Rev. Lett. **92**, 018303 (2004).
[42] S. A. Gurvitz and G. P. Berman, Phys. Rev. B **72**, 073303 (2005).
[43] H. J. Jiao, F. Li, S.-K. Wang, and X.-Q. Li, Phys. Rev. B **79**, 075320 (2009).
[44] J. Y. Luo, H. J. Jiao, J. Hu, X.-L. He, X. L. Lang, and S.-K. Wang, Phys. Rev. B **92**, 045107 (2015).
[45] A. Morello, J. J. Pla, F. A. Zwanenburg, K. W. Chan, K. Y. Tan, H. Huebl, M. Möttönen, C. D. Nugroho, C. Yang, J. A. van Donkelaar *et al.*, Nature (London) **467**, 687 (2010).
[46] J. P. Dehollain, J. T. Muhonen, K. Y. Tan, A. Saraiva, D. N. Jamieson, A. S. Dzurak, and A. Morello, Phys. Rev. Lett. **112**, 236801 (2014).
[47] Y. J. Yan, Phys. Rev. A **58**, 2721 (1998).
[48] S. A. Gurvitz and Y. S. Prager, Phys. Rev. B **53**, 15932 (1996).
[49] X. Q. Li, J. Y. Luo, Y. G. Yang, P. Cui, and Y. J. Yan, Phys. Rev. B **71**, 205304 (2005).
[50] F. Marquardt and C. Bruder, Phys. Rev. B **68**, 195305 (2003).
[51] B. Sothmann and J. König, Phys. Rev. B **82**, 245319 (2010).
[52] Y. J. Yan and R. X. Xu, Annu. Rev. Phys. Chem. **56**, 187 (2005).
[53] J. Y. Luo, H. J. Jiao, Y. Shen, G. Cen, X.-L. He, and C. Wang, J. Phys.: Condens. Matter **23**, 145301 (2011).
[54] J. Y. Luo, Y. Shen, X.-L. He, X.-Q. Li, and Y. J. Yan, Phys. Lett. A **376**, 59 (2011).
[55] D. Forster, *Hydrodynamics Fluctuations, Broken Symmetry, and Correlation Functions* (Benjamin, London, 1975).
[56] S. A. Gurvitz, Phys. Rev. B **56**, 15215 (1997).
[57] Y. Makhlin, G. Schön, and A. Shnirman, Phys. Rev. Lett. **85**, 4578 (2000).
[58] Y. Makhlin, G. Schön, and A. Shnirman, Rev. Mod. Phys. **73**, 357 (2001).
[59] A. C. Doherty, K. Jacobs, and G. Jungman, Phys. Rev. A **63**, 062306 (2001).
[60] J. S. Jin, X. Q. Li, and Y. J. Yan, Phys. Rev. B **73**, 233302 (2006).
[61] S. Pilgram and M. Büttiker, Phys. Rev. Lett. **89**, 200401 (2002).
[62] A. A. Clerk, S. M. Girvin, and A. D. Stone, Phys. Rev. B **67**, 165324 (2003).
[63] D. V. Averin and E. V. Sukhorukov, Phys. Rev. Lett. **95**, 126803 (2005).
[64] H. M. Wiseman and G. J. Milburn, Phys. Rev. A **47**, 1652 (1993).
[65] A. N. Korotkov, Phys. Rev. B **63**, 085312 (2001).
[66] A. N. Korotkov and D. V. Averin, Phys. Rev. B **64**, 165310 (2001).
[67] A. N. Jordan and M. Büttiker, Phys. Rev. Lett. **95**, 220401 (2005).
[68] B. Küng, O. Pfäffli, S. Gustavsson, T. Ihn, K. Ensslin, M. Reinwald, and W. Wegscheider, Phys. Rev. B **79**, 035314 (2009).
[69] D. V. Averin, Phys. Rev. Lett. **88**, 207901 (2002).
[70] A. N. Jordan and M. Büttiker, Phys. Rev. B **71**, 125333 (2005).
[71] J. Y. Luo, H. J. Jiao, B. T. Xiong, X.-L. He, and C. R. Wang, J. Appl. Phys. **114**, 173703 (2013).